https://doi.org/10.36375/prepare_u.iei.a221

SSR Stability Analysis and Modeling for DFIG Connected to Series Compensated Transmission Line

Neevatika Verma, Narendra Kumar
Department of Electrical Engineering
(Delhi Technological University)
(New Delhi-110042)
{nivetikaverma2311@gmail.com,}

Abstract - Due to the massive increase in electrical energy demand, wind power penetration into electric networks is increasing. Usually, the wind farms are located away from the grid, necessitating a series compensated transmission system. Series compensation is always prone to sub-synchronous resonance (SSR), which may lead to the torsional interactions resulting T-G shaft fatigue and associated protection system. In this paper, a modified IEEE first Benchmark Model is used for SSR analysis. A doubly-fed induction generator (DFIG) has been considered supplying power to the grid through a series compensated transmission line. The dynamics of the Rotor Side Converter (RSC) and the Grid Side Converter (GSC) is used to model the DFIG. Thus, it can generate a significant impact in system dynamics. However, previous works have considered a constant voltage source model for RSC and GSC. Therefore, consequently these models are not capable of replicating the dynamic impact of SSR for some critical factors. The inclusion of GSC and RSC modeling in analysis reflects dynamics that are more accurate. The eigenvalue analysis has been used to study the impact of SSR under different operating situations, for instance, wind speed fluctuations and varying the series compensation. To validate the analysis, time-domain simulations have been carried out by using MATLAB.

Keywords – Doubly Fed induction Generator (DFIG), Series Compensation, Sub-synchronous Resonance (SSR), Stability

INTRODUCTION

As renewable energy is the current requirement to meet the global power need without much impact on the environment. Wind power plays a significant role in fulfilling the power requirement. To accommodate the additional power, transmission infrastructural changes are frequently required for wind farms located far from load centers. From the economic considerations, series capacitor compensation of existing lines is typically recommended, over constructing new lines, to boost power transmission capacity and stability margin[1]. On the other hand, fixed series capacitor compensation is a source of SSR phenomenon not only in new power plants but also in existing generating power systems and power electronic equipment[2]. The primary source of the SSR phenomenon is the electrical resonance frequency, which is smaller in amplitude to the natural system frequency. It usually occurs if the natural mechanical frequency of the turbine matches with the electrical resonance frequency—the SSR oscillation results in the slip voltage of SSR frequency at the rotor circuit. The reason for the shaft failure is due to the oscillating electromagnetic torque, which consequently results in the failure of the shaft. This incident invites serious research on the SSR phenomenon in DFIGs and series compensated transmission lines[3].

The SSR phenomena were first discussed in 1937, and it resurfaced in the 1970s after two shaft collapses at the Mohave site received attention[4]. A decade ago, noticed the potential relationship between wind farms and series capacitors. Due to increasing levels of wind power, SSR occurrences have been observed in series-compensated DFIG based wind power plants (WPP) in the south of Texas, the southwest of Minnesota, and the north of China (Hebei province)[5]. Following the incidence, extensive research into the SSR problem among DFIGs and series-compensated power systems was conducted. According to reference [5], DFIGs are more susceptible to SSR in series compensated systems than fixed-speed wind turbine generators and wind generators connected via back-to-back converters.

Several previous research works discuss detailed mathematical modeling of a DFIG-based WPP[3],[6]–[10]. However, the RSC, GSC dynamics have not been considered for the

https://doi.org/10.36375/prepare_u.iei.a221

modeling and system analysis. The RSC and GSC have been considered to be a constant voltage source model[3],[7],[8] and a constant DC connection voltage amongst the RSC and the GSC. The RSC, as well as GSC must be simulated and included in the system modelling for internal dynamic analysis as they can introduce significant impact in the overall system dynamics. The dynamics of DFIG, RSC and GSC can be included in the stability analysis to improve its accuracy.

Now, because this modelling being more accurate, we have included the dynamics of RSC and GSC for overall system modeling and stability analysis via eigenvalue analysis as well as time-domain analysis in this work. The significant information regarding the damping of each mode and its oscillatory frequency can be achieved from the above analysis. The Eigenvalues enables to know the different modes of oscillations available in the complex electrical system

The whole paper is divided into the following sections: Section A discusses the detailed modeling of DFIG based WPP, which is linked with series compensated long-distance transmission line. The result and discussion part are given in section B, in which eigenvalue analysis, as well as time-domain analysis, is carried out. The conclusion is drawn in section C. In the last section, the Appendix shows the system parameters taken.

A. System modeling:

The IEEE first benchmark model has been adapted to analyze the SSR phenomenon in DFIG based wind energy conversion system instead of a synchronous generator integrated with a series compensated transmission line, as shown in Fig. 1[11]. A 161kV series compensated long transmission line connects an infinite bus to a 100MW DFIG based wind power plant (WPP) in this study. The DFIG has a 575 V rated voltage and a 60 Hz frequency. The 67 wind turbines that make up the 100-megawatt wind farm each having a 1.5MW capacity. In the Appendix, parameters for both the aggregated model and the single model are given.

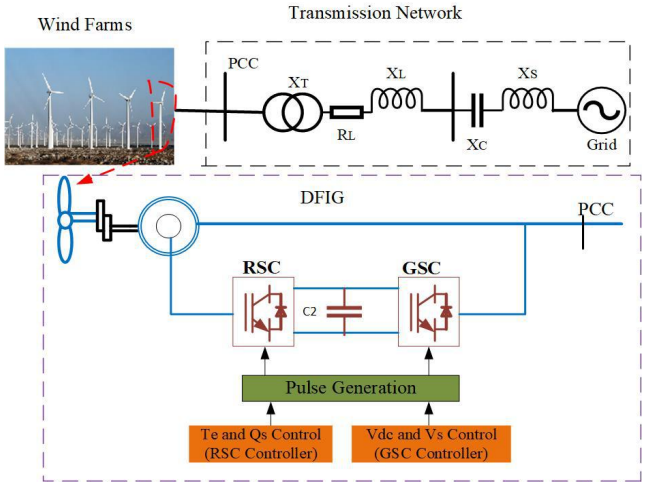

Fig. 1 IEEE first benchmark model of DFIG-based WPP

1) Modeling of wind turbine: A wind turbine's mechanical output torque is proportional to the wind speed and can be expressed as:

$$Tm = \frac{\rho R A C_p V_{wi}^2}{2\lambda} \quad (1)$$

Where ρ represents the air density(kgm^{-3}), R defines wind turbine rotor radius(m), A denotes the blade sweep area(m^2), V_{wi}^2 signifies the wind speed(m/s), and C_p denotes the blade power coefficients, which is determined by the blade pitch angle θ and tip speed ratio as fallow:

$$C_p = 0.5\left(\frac{RC_f}{\lambda} - 0.022\theta - 2\right) e^{-0.255\left(\frac{RC_f}{\lambda}\right)} \quad (3)$$

The tip speed ratio is expressed as:

$$\lambda = \frac{\Omega_m R}{V_{wi}} \quad (4)$$

Ω_m denotes the mechanical angular velocity (rad/s)

Fig. 2 depicts the link between mechanical power, rotor speed (pu), and wind speed for a 1.5MW wind turbine when the pitch angle θ is zero with 200ft rotor radius is assumed.

https://doi.org/10.36375/prepare_u.iei.a221

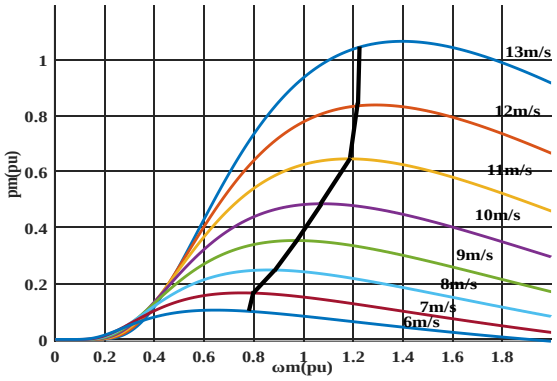

Fig. 2 relationship between wind power wind speed and rotor speed

We can develop a lookup table as shown in Table 1 that lists the various wind speeds and the rotor speed, maximum mechanical power, and shaft torque. It should be emphasized that in the small-signal analysis technique, Table 1 depicts the wind turbine model. This Table, by including a torque control loop, can obtain the desired optimum rotor speed.

TABLE I
Mechanical Power, Torque, Rotor Speed (Pu), and Wind Speed

V_{wi}	7m/s	8m/s	9m/s	10m/s	11m/s	12m/s
ω_m	0.8	0.88	0.97	1.06	1.18	1.2
P_m	0.24	0.28	0.39	0.47	0.64	0.84
T_m	0.3	0.32	0.4	0.46	0.54	0.7

2) Modelling of Shaft System: The two-mass system often represents torsional dynamics in power system analysis. The first mass is represented by wind turbine shaft, which has a low speed, and a DFIG high-speed shaft system represents the second mass system; and A two-mass system's state-space representation is as follows:

$$\frac{d}{dt}\begin{bmatrix}\omega_t\\ \omega_r\\ T_g\end{bmatrix}=\begin{bmatrix}\frac{-D_t-D_{tg}}{2H_t} & \frac{D_{tg}}{2H_t} & \frac{-1}{2H_t}\\ \frac{D_{tg}}{2H_g} & \frac{-D_g-D_{tg}}{2H_g} & \frac{1}{2H_g}\\ K_{tg}\omega_g & -K_{tg}\omega_e & 0\end{bmatrix}\begin{bmatrix}\omega_t\\ \omega_r\\ T_g\end{bmatrix}+\begin{bmatrix}\frac{T_m}{2H_t}\\ \frac{-T_e}{2H_t}\\ 0\end{bmatrix} \quad (5)$$

The wind turbine, DFIG rotor speed, and internal torque of the model are represented by state variablesω_t, ω_r and T_g , respectively.T_m and T_e are the mechanical and electromagnetic torque of the generator, respectively, and these are shaft system models of the input side. D_t and H_t are the damping coefficient and inertia constant of the wind turbine, respectively, and H_g is the inertia constant of the wind generator. D_{tg} and K_{tg} are the damping coefficient and shaft stiffness of the coupling between two masses; these are the constant of a two-mass model system. The optimal wind turbine torque T_m is obtained from table1 at any required wind speed, whereas T_e it could be written as air gap flux leakage and currents of the DFIG is express:

$$T_e=\Psi_{qm}i_{dr}-\Psi_{dm}i_{qr} \quad (6)$$

$$\Psi_{qm}=X_m(i_{qs}+i_{qr}) \quad (7)$$

$$\Psi_{dm}=X_m(i_{ds}+i_{dr}) \quad (8)$$

3) Modelling of DFIG

The modelling of DFIG with rotor side converter, a dynamic model of the sixth order is used. The model is characterized as**:**

$$\dot{x}=A_DX_D+B_DU_D \quad (9)$$

where the state variables are denoted by X_D, U_D denotes the inputs of DFIG, B_D denotes the constants of electrical parameter, and A_D Represents the constants of state variables.

$$X_D=[i_{qs};\ i_{ds};\ i_{0s};\ i_{qr};i_{dr};i_{0r};] \quad (10)$$

$$U_D=[v_{qs};v_{ds};v_{0s};v_{qr};v_{dr};v_{0r};] \quad (11)$$

The subscripts s, r, d, q, and 0 signify the stator and rotor sides, respectively, as well as direct, quadrature, and zero sequences. The parameters i0s, i0r, v0s, and v0r are equal to zero because the system is balanced.

$A_D$and $B$is expressed as:

$$A_D=-B_D\begin{bmatrix}R_S & \frac{\omega_s}{\omega_b}X_s & 0 & 0 & \frac{\omega_s}{\omega_b}X_m & 0\\ -\frac{\omega_s}{\omega_b}X_s & R_S & 0 & -\frac{\omega_s}{\omega_b}X_m & 0 & 0\\ 0 & 0 & R_S & 0 & 0 & 0\\ 0 & \frac{\omega_s-\omega_r}{\omega_b}X_m & 0 & R_r & \frac{\omega_s-\omega_r}{\omega_b}X_r & 0\\ -\frac{\omega_s-\omega_r}{\omega_b}X_m & 0 & 0 & -\frac{\omega_s-\omega_r}{\omega_b}X_r & R_r & 0\\ 0 & 0 & 0 & 0 & 0 & R_r\end{bmatrix}$$

$$B_D=\omega_b\begin{bmatrix}X_s & 0 & 0 & X_m & 0 & 0\\ 0 & X_s & 0 & 0 & X_m & 0\\ 0 & 0 & X_{ls} & 0 & 0 & 0\\ X_m & 0 & 0 & X_r & 0 & 0\\ 0 & X_m & 0 & 0 & X_r & 0\\ 0 & 0 & 0 & 0 & 0 & X_{lr}\end{bmatrix}^{-1} \quad (12)$$

Except for ω_b, ω_r, and ω_s, which are in rad/sec, all parameters and variables are in per-unit.

https://doi.org/10.36375/prepare_u.iei.a221

4) Modelling of DC link: A first-order model describes the dynamics of the capacitor in the dc link between the GSC and the RSC.

$$C_{dc}V_{dc}\frac{dV_{dc}}{dt} = P_r - P_g \quad (13)$$

$$P_r = \frac{1}{2}\left(v_{qr}i_{qr} + v_{dr}i_{dr}\right) \quad (14)$$

$$P_g = \frac{1}{2}\left(v_{qg}i_{qg} + v_{dg}i_{dg}\right) \quad (15)$$

The RSC and GSC's active powers are P_r and P_g, respectively. V_{dc} is the actual value whereas, $v_{qr}, i_{qr}, v_{dr}, i_{dr}, v_{qg}, i_{qg}, v_{dg}, i_{dg}$ are in per-unit.

5) Series compensated transmission line Modeling: Generally, the dynamics of the series compensated model are ignored, but SSR analysis is essential. The transmission line can be electrically depicted as lumped series RLC circuit and adopts the synchronous reference frame to modeling the series compensated transmission line. Per phase dynamics equations is expressed as:

$$R_l.i_l + L\frac{di_l}{dt} + v_c = v_s - V_B \quad (16)$$

$$C\frac{dv_c}{dt} = i_l \quad (17)$$

The compensated transmission's state-space representation is expressed as:

$$\frac{d}{dt}\begin{bmatrix} i_{ql} \\ i_{dl} \\ v_{cq} \\ v_{cd} \end{bmatrix} = \begin{bmatrix} -\frac{R_l}{X_l} & -\omega_e & -\frac{1}{X_l} & 0 \\ -\omega_e & -\frac{R_l}{X_l} & 0 & -\frac{1}{X_l} \\ X_c & 0 & 0 & -\omega_e \\ 0 & X_c & \omega_e & 0 \end{bmatrix}\begin{bmatrix} i_{ql} \\ i_{dl} \\ v_{cq} \\ v_{cd} \end{bmatrix} + \omega_b \begin{bmatrix} \frac{v_{qs}-V_{Bq}}{X_l} \\ \frac{v_{ds}-V_{Bd}}{X_l} \\ 0 \\ 0 \end{bmatrix} \quad (18)$$

Where i_{dl} i_{ql} is the transmission line's direct and quadrature axis current, respectively, and v_{cd} are the quadrature also direct axis voltage across the capacitor. The Voltage's quadrature and direct axes of the infinite are V_{Bq} and V_{Bd}, respectively. The synchronous reference speed and the base speed are both 1pu or 377rad/s.

6) *6) Modeling of DFIG converter:* This study aims to look at both RSC and GSC converter controllers. Vector-controlled techniques is adopted in this study. The control loop is shown in Fig.2 and Fig.3. For the RSC controller, Table1 is used for the obtain the optimal reference torque. When the wind speed exceeds the rated speed, the value remains constant. When the wind speed is less than the rated speed, the reference torque is the torque that provides the maximum rotational speed at the measured rotational speed. Using this lookup table, the wind turbine can extract the maximum amount of wind energy feasible.

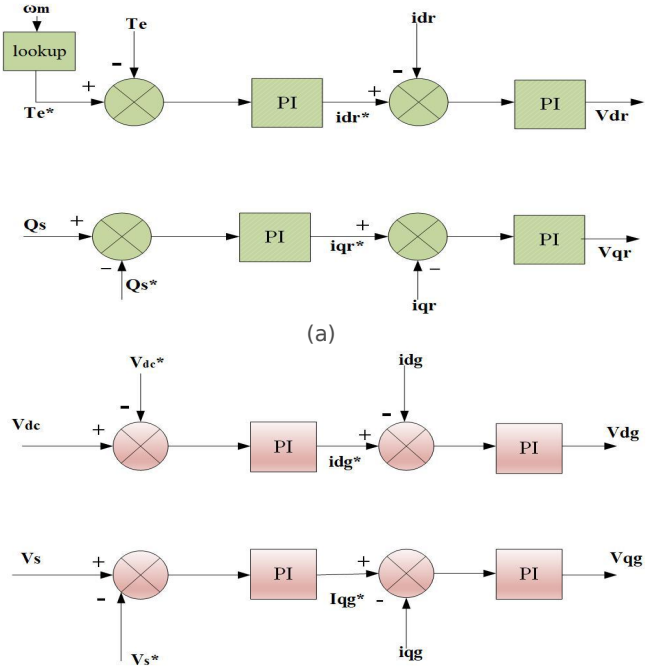

Fig. 3 (a) RSC, (b) GSC control loop

) *7) Integrated system modelling:* To understand the complete system, it is useful to think of it as an integration of the various subsystems. Equation expresses the entire system model (25).

$$[\dot{X}] = [A_{sys}][X_{sys}] + [B_{sys}][U_{sys}] \quad (19)$$

Where $[X_{sys}] = [X_{shaft}\, X_{DFIG}\, X_{tl}\, X_{dc}]$ (20)

The system matrix of the entire system is given by

$$[A_{sys}] = \begin{bmatrix} A_{shaft} & 0 & 0 & 0 \\ 0 & A_{DFIG} & 0 & 0 \\ 0 & 0 & A_{tl} & 0 \\ 0 & 0 & 0 & A_{dc} \end{bmatrix} \quad (21)$$

These interconnected subsystems are able to communicate with each other via state and control variables in the individual subsystems. Algebraic Equations of v_{ds}, v_{qs}, i_{ds} and i_{qs} are used to link the controllers. Now v_{ds}, v_{qs}, i_{ds} and i_{qs} expressed as:

$$v_{ds} = v_{dg} + X_{tg}i_{qg} \quad (22)$$

$$v_{qs} = v_{qg} + X_{tg}i_{dg} \quad (23)$$

$$i_{ds} = i_{dg} - i_{dl} \quad (24)$$

$i_{qs}=i_{qg}-i_{ql}$
(25)
Developed torque and stator reactive power is given by:
$T_g = X_m\left(i_{dr}i_{qs}-i_{ds}i_{qr}\right)$
(26)
$Q_s=\frac{1}{2}\left(v_{qs}i_{ds}-v_{ds}i_{qs}\right)$
(27)
A state-space model is used to investigate the system's small signal stability, which leads to time-domain simulation analysis and eigenvalue computation.

B. Result and discussion

A) *Eigen value analysis:* The eigenvalue approach is one of the most critical approaches for studying a dynamic system's small-signal stability. Based on the order of the system matrix, this analysis generates a collection of eigenvalues. The eigen values can be used to determine a system's stability; if the real component of an eigen value is positive, the system is unstable; if the real part is negative, the system is stable. The frequency of oscillations is represented by the imaginary portion. The size of the system matrix (A_{sys}) is determined in Section A, which is the 22x22 size of the matrix, resulting in 22 eigenvalues. By varying the wind speed and compensation level of a transmission line, different eigen values can be determined. Table II displays the set of eigenvalues (from λ_1 to λ_{22}) for fixed wind speeds at 7m/sand at a constant capacitive compensation level of 50%. As shown in Table II, the eigenvalues λ5 and λ6 are found unstable at these operating circumstances, and the system becomes increasingly unstable.

The remaining computed eigenvalues operate in a variety of ways. Electromechanical modes with eigen values of λ_7,-λ_{12} are reported to be responsible for electromechanical system dynamics. λ_1,λ_2, and λ_3,λ_4 belong to the extremely high frequency and super synchronous modes, respectively, because the frequency of these dynamics is higher than the system's, they are always stable. The λ_{13},λ_{22} do not have any frequency terms and are classified as oscillatory as positive modes or non-oscillatory as a negative mode, with amplitudes which are variable as a function of compensation levels as well as wind speeds. As compensation increases, the real part of λ_5,λ_6 grows in size, and the system becomes increasingly unstable, as seen in Table III. The system stability is observed to be dependent on the percentage of compensation offered to the transmission line based on the eigenvalues. The system gets more stable as the wind speed increases. The time-domain simulation of this system, as well as the RSC and GSC controllers, are detailed in the next section.

TABLE II
EIGEN VALUE ANALYSIS OF THE COMPLETE SYSTEM MODEL WITH 50% COMPENSATION AND A WIND SPEED OF 7 M/S

Mode	Eigenvalue	Frequency (Hz)	Description
$\lambda_{1,2}$	$-1790\pm j889$	141	Very high freq.
$\lambda_{3,4}$	$-19.2\pm j568.2$	90.4	Sup-sync
$\lambda_{5,6}$	**$1.6\pm j187.8$**	**29.9**	**SSR**
$\lambda_{7,8}$	$-52.4\pm j7.9$	1.25	Electromech.
$\lambda_{9,10}$	$-0.63\pm j18.8$	2.86	Electromech.
$\lambda_{11,12}$	$-6.41\pm j8.6$	1.36	Electromech.
$\lambda_{20,21}$	$-0.0\pm j0.0$	0	PI Controller
λ_{13}	5.9	0	No oscillatory
λ_{14}	-7.4	0	No oscillatory
λ_{15}	-5.8	0	No oscillatory
λ_{16}	-5.6	0	No oscillatory
λ_{17}	1.9	0	No oscillatory
λ_{18}	-48.2	0	No oscillatory
λ_{19}	-37.7	0	No oscillatory
λ_{22}	-0.0	0	No oscillatory

TABLE III
EIGEN VALUE ANALYSIS OF MODE 3($\lambda_{5,6}$) AT VARYING WIND SPEED AND % OF SERIES COMPENSATION

%Compensation	Wind Speed	Mode3 ($\lambda_{5,6}$)	
		Eigen value	Frequency (Hz)
40	7m/s	**$0.01\pm j207$**	32.96
	9m/s	$0.04\pm j206.9$	32.94
	11m/s	$0.12\pm j206.8$	32.92
50	7m/s	**$1.6\pm j187.8$**	29.90
	9m/s	**$1.5\pm j187.7$**	29.88
	11m/s	**$1.4\pm j187.5$**	29.85
60	7m/s	**$3.2\pm j170.9$**	27.21
	9m/s	**$3.1\pm j170.7$**	27.18
	11m/s	**$2.9\pm j170.4$**	27.13

https://doi.org/10.36375/prepare_u.iei.a221

B) Time-domain analysis: MATLAB/Simulink has been used for the time-domain analysis to verify the results of eigenvalue analysis. At a constant wind speed (7 m/s), Fig. 4 displays the Pe electrical dynamic response with various compensation values. The dynamic reaction is initiated when the compensation level of 40% is increased to 50% and 60%, respectively, at time t=2s. At a specific wind speed (9 m/s), Fig. 5 displays the Pe electrical dynamic response with various compensation values. As illustrated in Fig.4 and 5, The damping decreases as the compensating level rises. The result reveals that as the compensation level is raised, the SSR frequency rises while the damping decreases. As seen in Fig. 5, the SSR damping improves with increasing wind speed.

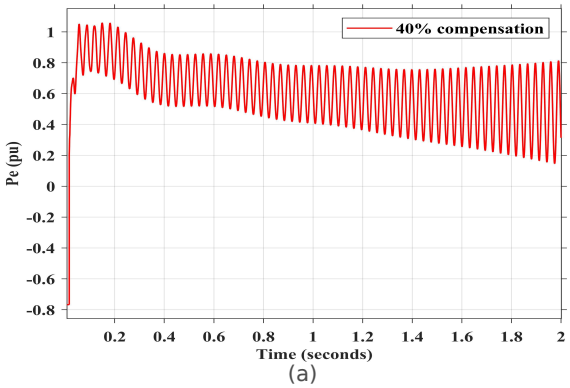

(a)

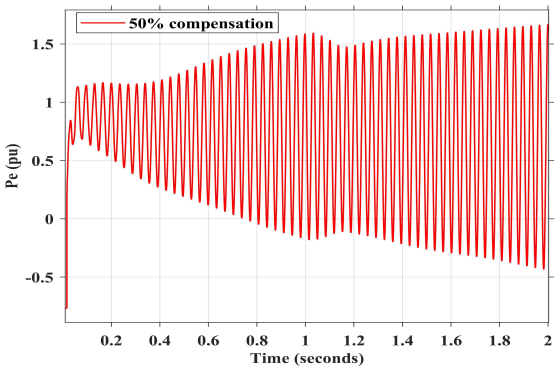

(b)

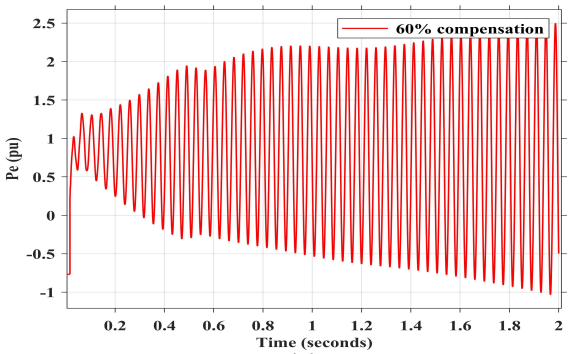

(c)

Fig. 4 Electrical power dynamics response at (a)40%, (b) 50% and (c) 60% compensation at fixed wind speed 7m/s

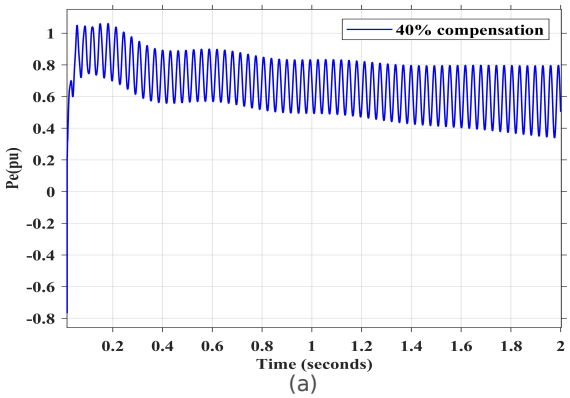

(a)

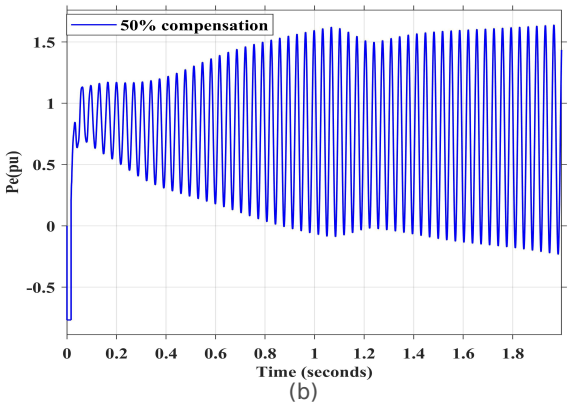

(b)

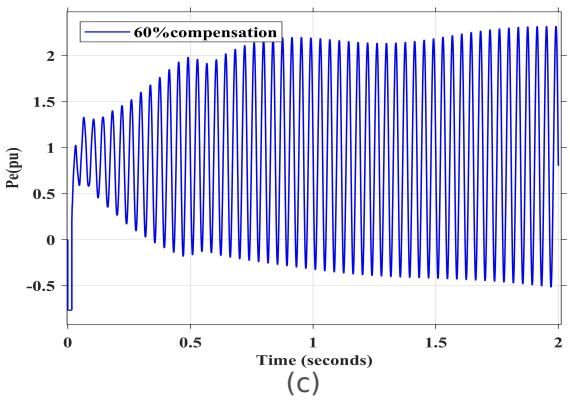

(c)

Fig. 5 Electrical power dynamics response at (a)40%, (b) 50% and (c) 60% compensation at fixed wind speed 9m/s

As a result, the system becomes unstable at a wind speed of 7 m/s due to the negative damping of the oscillation. The system is stable at greater wind speeds. These findings are consistent with the notion that the dominant mode becomes more unstable when wind speed falls.

C. Conclusion

For the small-signal stability investigation, a detailed mathematical model of the 100MW grid-connected DFIG based WPP based on the IEEE first benchmark model, as well as a dynamic model of the RSC and GSC converters, has been done. The numerous modes of oscillations present in the integrated system can be easily discovered using eigenvalue analysis. The stability of the various oscillating modes can be identified by analysing the nature of eigenvalues. In MATLAB/Simulink, oscillations present in the electromagnetic torque produced for various compensation levels are investigated, and the eigenvalue analysis is validated. In this paper, SSR analysis has been carried out using an eigenvalue technique for various wind speeds and capacitance compensation levels and got different oscillation modes, and the above result has been validated using time-domain analysis. The fallowing conclusion has obtained:

- The real component magnitude of the eigenvalue increases as the fraction of series compensation is raised, and the system becomes increasingly unstable.
- The increase in wind speed velocity decreases the amplitude of the real part of eigen value, resulting in a better stable system.

APPENDIX

TABLE IV
DFIG PARAMETERS

Rated power	1.5MW	100MW
Rated Voltage	575V	575V
Rated Frequency	60Hz	60Hz
R_S	0.023	0.023
X_{lS}	0.18	0.18
R_r	0.016	0.016
X_{lr}	0.16	0.16
X_M	2.9	2.9
DC-link voltage	1200V	1200V
DC-link capacitor	10000μF	67*10000μF

TABLE V
TRANSMISSION LINE PARAMETERS

Transformer Ratio	575V/161kV
Base power	100MVA
R_l	0.02
X_l	0.5
X_C at 50% compensation level	64.8 ohm
X_T	0.14
X_{sys}	0.06

TABLE IV
DRIVE TRAIN PARAMETERS

H_t	4.32 sec
H_g	0.685 sec
D_t	0
D_g	0
D_{tg}	1.5 p. u
K_{tg}	1.11

TABLE V
PI PARAMETERS OF DFIG CONVERTER

K_{P1}	0.2	K_{i1}	0.4
K_{P2}	4	K_{i2}	100
K_{P3}	0.01	K_{i3}	0.04
K_{P4}	4	K_{i4}	100
K_{P5}	0.1	K_{i5}	2
K_{P6}	0.08	K_{i6}	0.5
K_{P7}	0.1	K_{i7}	2
K_{P8}	0.08	K_{i8}	0.5

REFERENCES

[1] M. Khayyatzadeh and R. Kazemzadeh, “Sub-synchronous resonance damping using high penetration PV plant,” *Mech. Syst. Signal Process.*, vol. 84, pp. 431–444, 2017.

[2] G. Li *et al.*, “Analysis and Mitigation of Subsynchronous Resonance in Series-Compensated Grid-Connected System Controlled by a Virtual Synchronous Generator,” *IEEE Trans. Power Electron.*, vol. 35, no. 10, pp. 11096–11107, 2020.

[3] L. Fan, R. Kavasseri, Z. L. Miao, and C. Zhu, “Modeling of DFIG-based wind farms for SSR analysis,” *IEEE Trans. Power Deliv.*, vol. 25, no. 4, pp. 2073–2082, 2010.

[4] A. Adrees, *Risk Based Assessment of Subsynchronous Resonance in AC/DC Systems*. 2017.

[5] J. Shair, X. Xie, L. Wang, W. Liu, J. He, and H. Liu, “Overview of emerging subsynchronous oscillations in practical wind power systems,” *Renew. Sustain. Energy Rev.*, vol. 99, no. September 2018, pp. 159–168, 2019.

[6] J. B. Ekanayake, L. Holdsworth, X. G. Wu, and N. Jenkins, “Dynamic modeling of doubly fed induction generator wind turbines,” *IEEE Trans. Power Syst.*, vol. 18, no. 2, pp. 803–809, 2003.

[7] Y. Lei, A. Mullane, G. Lightbody, and R. Yacamini, “Modeling of the wind turbine with a doubly fed induction generator for grid integration studies,” *IEEE Trans. Energy Convers.*, vol. 21, no. 1, pp. 257–264, 2006.

[8] H. A. Mohammadpour, A. Ghaderi, and E. Santi, “Analysis of sub-synchronous resonance in doubly-fed

https://doi.org/10.36375/prepare_u.iei.a221

induction generator-based wind farms interfaced with gate – controlled series capacitor," *IET Gener. Transm. Distrib.*, vol. 8, no. May, pp. 1998–2011, 2014.

[9] A. S. Trevisan *et al.*, "Analysis of low frequency interactions of DFIG wind turbine systems in series compensated grids," *Electr. Power Syst. Res.*, vol. 191, no. February 2020, p. 106845, 2021.

[10] J. Shair, X. Xie, W. Liu, X. Li, and H. Li, "Modeling and stability analysis methods for investigating subsynchronous control interaction in large-scale wind power systems," *Renew. Sustain. Energy Rev.*, vol. 135, no. August 2020, p. 110420, 2021.

[11] P. S. E. C. IEEE, "IEEE Subsynchronous Resonance Task Force of the Dynamic System Performance Working Group Power System Engineering," *IEEE Trans. Power Appar. Syst.*, vol. PAS-96, no. 5, pp. 1565–1572, 1977.